J Mater Sci (2007) 42:692–698
DOI 10.1007/s10853-006-0282-6

Improved microstructural features in screen printed NdBCO thick films on YSZ substrates

M. A. Moussa · J. S. Abell · T. C. Shields

Received: 17 June 2005 / Accepted: 12 October 2005 / Published online: 28 October 2006

Abstract An investigation of the effect of using Ba-rich precursors, $Nd_{0.9}Ba_{2.1}Cu_3O_y$ + 15 wt% $Nd_{3.6}Ba_{2.4}Cu_{1.8}O_z$, on the melt growth, microstructure and superconducting properties of NdBCO screen-printed thick films on YSZ substrates has been carried out. The presence of unreacted powder ($BaCuO_2$) in the precursor increased the amount of liquid and resulted in the formation of a large grain size. However, the addition of Nd_{422} was effective in stabilising the liquid viscosity at the processing temperature and reducing the film/substrate interaction. As a consequence, high transition temperatures and sharp superconducting transitions were obtained. It has been found that the cooling rate affects the texture orientation, grain size and quality in addition to the interaction between the film and the substrate. The magnetic flux dynamics have been investigated using the Magneto-Optical (MO) technique at various low temperatures and different external applied magnetic fields. The magnetization critical current density was 4.1×10^4 A/cm^2 at 5 K and zero field.

Introduction

The superconducting thick film route is considered the easiest and cheapest alternative technology to vacuum deposition thin film route. Although the superconducting properties of thin films are incomparable, thick films fabricated by the non-vacuum screen printing technique have the advantages of being comparatively easy to fabricate and can cover relatively large areas. The screen-printing technique has been widely used for the fabrication of $YBa_2Cu_3O_{7-\delta}$ (YBCO) high-temperature superconducting thick films [1–4] and there are many practical applications for these films. For example, YBCO thick films have been used in receiver coils for very low field magnetic resonance imaging (MRI) [5, 6], fault current limiters [7] and magnetic shielding [8]; microwave devices like antennas [9], resonators and filters [10]. This makes the optimization of the thick film route, especially screen-printed films, important for the growth of the superconducting electronics industry.

The $NdBa_2Cu_3O_x$ (NdBCO) system has many valuable superconducting properties compared with other systems, such as YBCO. It is characterized by T_C values of up to 96 K, a critical current density (J_C) of up to 1.2×10^5 A/cm^2 at 77 K and 2.5 T and irreversibility fields exceeding 13 T at 77 K, which can be achieved for NdBCO bulk materials [11, 12]. The NdBCO system has a higher growth rate; about 50 times the growth rate of the YBCO system [13]. This is due to the fact that the NdBCO peritectic decomposition temperature (T_P) is 60 °C higher than that of YBCO [14] and the dissolution and solubility of Nd in the ternary liquid is much higher than that of Y [15].

One of the most important features of the NdBCO system in comparison with YBCO is the formation of a solid solution, $Nd_{1+x}Ba_{2-x}Cu_3O_z$ (Nd_{123SS}), associated with the large ionic radius of the Nd^{+3} ions, which is close to that of Ba^{+2}. It has been found that the value

M. A. Moussa (✉)
Faculty of Science, Physics Department, Mansoura University, Mansoura 35516, Egypt
e-mail: moussa1864@mans.eg

J. S. Abell · T. C. Shields
School of Metallurgy and Materials, Birmingham University, Birmingham B15 2TT, UK

of the solubility limit (x) has a great effect on the properties of the NdBCO system; a low T_C and broad superconducting transition were found for large values of x ($x > 0.1$) [16]. The value of x depends on the starting composition, temperature and the oxygen partial pressure [17]. Consequently, to overcome the solid solution problem in NdBCO bulk material, the processing must be carried out under reduced oxygen atmosphere (0.1–1% O_2 in Ar) [18]. The NdBCO phase, which is prepared by this oxygen-controlled melt growth (OCMG) technique, has a high T_C and sharp superconducting transition. A second method of dealing with the solid solution formation is Ar annealing at a high temperature after processing the bulk material in air [19, 20]. Another way is to increase the Ba ratio by the addition of a Ba-rich phase such as Nd_2BaO_4 or Nd_{422} ($Nd_{4-2x}Ba_{2+2x}Cu_{2-x}O_z$) phase [21].

However, in the fabrication of NdBCO thick films [22, 23] the high T_P has resulted in a decrease in the liquid viscosity and a severe film/substrate interaction, degrading the superconducting properties. Moreover, the presence of large amounts of liquid phase during the processing of the NdBCO system due to the higher dissolution/solubility of Nd ion in the ternary liquid has also hindered the successful fabrication of NdBCO thick films.

It has been found that the addition of 10 wt% Ba-rich Nd_{422} phase to Ba-rich or to stoichiometric NdBCO starting powders, was useful in stabilising the liquid viscosity and producing dense thick films on polycrystalline yttria stabilized zirconia (YSZ) substrates [24, 25]. The screen-printed thick films which were fabricated with this addition have an improved microstructure, high-T_C and sharp superconducting transition. However, these films were characterized by a surface morphology of small square grains and low J_C values. It is well known that the presence of un-reacted powder in the starting precursor from which screen-printed YBCO thick films are fabricated (and/or processing under He gas atmosphere) increases the amount of liquid and promotes large grain growth [26]. The large grain growth (hub and spoke) and the better connectivity between them have resulted in relatively high J_C values [27].

The aim of this paper is to report the use of a $Nd_{0.9}Ba_{2.1}Cu_3O_y$ + 15 wt% Ba-rich Nd_{422} ($Nd_{3.6}Ba_{2.4}Cu_{1.8}O_y$) mixed phase starting powder for the fabrication of NdBCO thick films on YSZ substrates. The Ba-rich Nd_{123} phase was designed to provide a relatively large amount of un-reacted powder which would enhance liquid phase formation and help in increasing the NdBCO grain size and increase J_C values. The addition of 15 wt% Ba-rich Nd_{422} to the powder was to compensate for the decrease in the viscosity of the melt at the high processing temperature and to be a source of Ba. Thick films were processed in 0.1% O_2 in Ar to reduce the T_P and hence reduce the film/substrate interaction.

Experimental

The precursor powders were prepared from Nd_2O_3, $BaCuO_2$ and CuO. The preparation details of the $Nd_{0.9}Ba_{2.1}Cu_3O_x$ precursor can be found elsewhere [24]. After weighing with the cationic ratio Nd: Ba: Cu = 0.9:2.1:3 and intimately mixing using zirconia balls in ethanol for 24 h, the mixture was dried and put in an alumina boat in a calibrated tube furnace and calcined at 820 °C under $p(O_2)$ = 1.0% O_2 in Ar (flow rate 400 ml/min) for 12 h. The last step was repeated at 840 °C for 12 h after grinding. The product was reground and checked for phase purity by X-ray diffraction (XRD). The Ba-rich phase Nd_{422} ($Nd_{3.6}Ba_{2.4}Cu_{1.8}O_z$) was prepared by the same method but also calcined at 860 °C and 900 °C for 36 h in 1% O_2 in Ar. $Nd_{0.9}$ $Ba_{2.1}$ Cu_3O_y + 15 % $Nd_{3.6}Ba_{2.4}Cu_{1.8}O_z$ were mixed and calcined at 860 °C for 16 h in 1% O_2 in Ar.

The ink was prepared from the precursor powders by mixing 4 g with 1 g organic binder ME105/5 (80% solid to 20% binder). Tracks of 25 mm × 5 mm were screen printed onto YSZ substrates to a total green thickness of 90–100 μm. After each pass, the produced film was dried for 20 min at 100 °C before the next layer was printed.

The atmosphere during subsequent firing was adjusted by two electronic mass flow controllers (Tylan FC 2900, 600 SCCM), which were controlled by an ROD-4 controller. They were used to mix 1% O_2 in Ar with Ar to produce 0.1% O_2 in Ar. This technique was used in the calcination and processing of the thick films. An oxygen monitor (Weldox) was used to monitor the value of $p(O_2)$.

Thick films were processed in 0.1% O_2 atmosphere with the following thermal programme. The furnace was ramped up to 600 °C in pure oxygen (400 ml/min) with a heating rate 300 °C/h to burn off the binder. The temperature was held for 1 h then the oxygen gas was replaced by 0.1% O_2 in Ar and held at that temperature for another 1 h to achieve a steady state of 0.1% O_2 atmosphere. The processing temperature was increased to 1036 °C with heating rate 5 °C/min, held for 6 min and then cooled by 180 °C/h to 990 °C. Different cooling rates (140, 120, 100, 80, 60, 40 and 20 °C/h) were used between 990 °C and 750 °C, followed by furnace cooling to room temperature. These melt

processed films were then annealed in flowing pure oxygen according to the following regime. The furnace was ramped up to 500 °C, held for 1 h, then, slowly cooled to 300 °C over 2 days and held for 120 h before the furnace cooling to room temperature.

The superconducting properties of the films were examined using AC susceptibility and DC transport critical current (77 K) methods. Four point transport measurements were taken on the standard 25 mm × 5 mm tracks using silver wires on silver contact pads. The silver dag pads were annealed in pure oxygen for 1 h at 500 °C, the wires were attached with more dag and then dried at 100 °C for 5 h. The microstructural characteristics of the processed films were examined using XRD, optical microscopy and scanning electron microscopy (JEOL 6300 SEM) fitted with energy despersive X-ray (EDX) analysis. Magneto-Optic (MO) imaging was used to observe magnetic flux dynamics and weak-links in processed films at different temperatures and different applied magnetic fields. Magnetization measurements were taken on an Oxford vibrating sample magnetometer (VSM) in the field range 0–1.5 T and temperature range 5–50 K.

Results and discussion

Microstructure

Since T_p of NdBCO is high compared with that of YBCO, processing NdBCO thick films on YSZ without the addition of Nd_{422} has led to substantial liquid loss and formation of porous film surfaces [24]. This morphology has been found for thick films processed at both high and low temperatures by processing under 1% O_2 in Ar or 0.1% O_2 in Ar, respectively. But the addition of the Nd_{422} phase to the precursor was effective in stabilising the liquid viscosity and producing dense and less porosity films. Fig. 1 shows the XRD pattern of the precursor which was used in the fabrication of NdBCO thick films on YSZ substrates. As can be seen, the main phase is the NdBCO phase. However, the calcination at low temperatures 820 °C and 840 °C for a short time (12 h) resulted in the formation of a relatively large amount of un-reacted powder ($BaCuO_2$). The XRD patterns of NdBCO thick films processed at 1036 °C under 0.1% O_2 in Ar and cooling rates 140, 100, 60 and 20 °C/h are shown in Fig. 2. In addition to the main phase Nd_{123} which is indexed, weak peaks were ascribed to Nd_{422}, CuO and YSZ substrate phases. The peaks of the Nd_{422} phase were detected in all the films but they were slightly

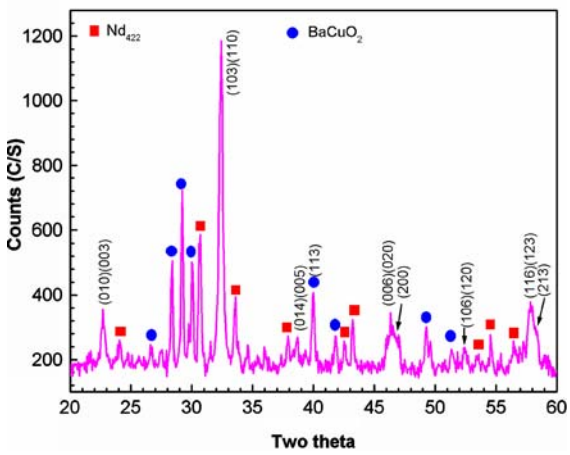

Fig. 1 XRD pattern of the $Nd_{0.9}Ba_{2.1}Cu_3O_x$ + 15 wt% $Nd_{3.6}Ba_{2.4}Cu_{1.8}O_y$ powder used in the fabrication of screen-printed thick films

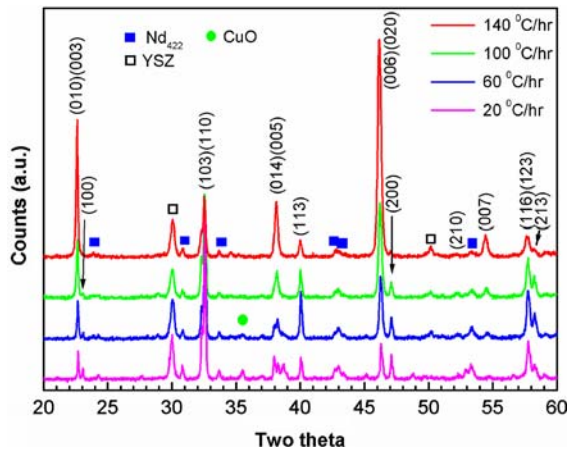

Fig. 2 XRD patterns of NdBCO thick films processed by cooling rates 140, 100, 60 and 20 °C/h

stronger with slower cooling rates. Thick films processed by fast cooling rates show a large degree of *c*-axis texturing. As the cooling rates become slower the degree of texturing (00() decreases and (*h*00) reflections increase.

The surface of processed thick films are characterized by two types of NdBCO crystal grain growth. The first one involves a Nd_{123} crystallites with the *c*-axis oriented perpendicular to the surface of the substrate, which can be defined as perpendicular *c*-axis grain growth. The second type has Nd_{123} crystallites with the *c*-axis making an angle with the normal on the substrate (inclined *c*-axis grain growth). Figure 3a, b show SEM surface images of the film which was prepared by a cooling rate of 140 °C/h. This relatively fast cooling rate has resulted in the formation of Nd_{123} small platelets with their *c*-axis normal to the substrate surface (see Fig. 2). With a slower cooling rate (60 °C/h),

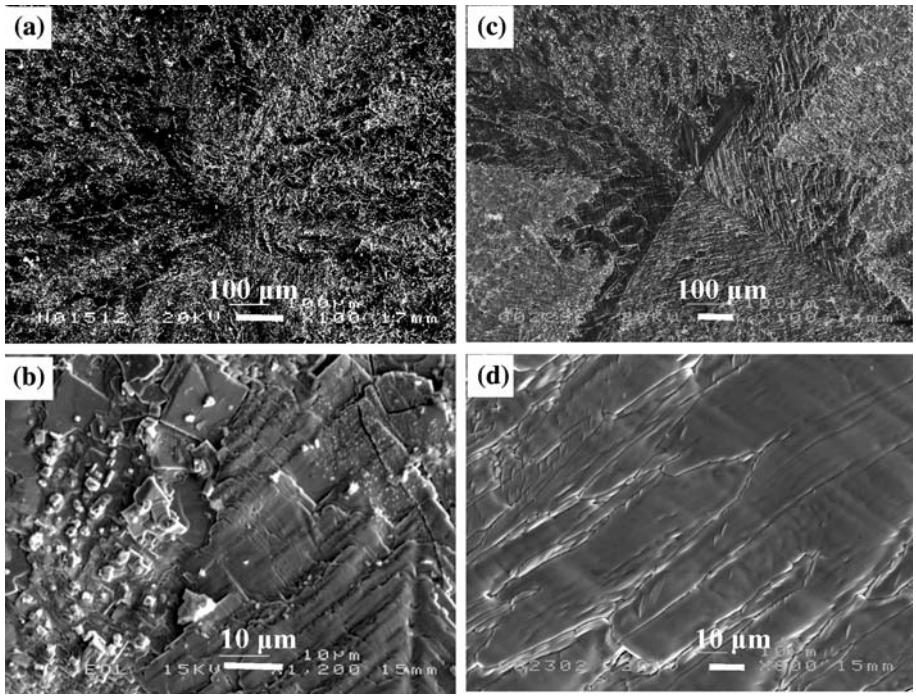

Fig. 3 SEM surface images of NdBCO thick films prepared by cooling rates 140 and 60 °C/h: 140 °C/h (**a**) and (**b**); 60 °C/h (**c**) and (**d**)

the Nd_{123} crystallite sizes increase as can be seen in Fig. 3c, d. Although the Nd_{123} crystallites have larger sizes their orientations correspond to inclined *c*-axis grain growth.

A relatively large crystallite size 3.5 $mm^2 \times 2.5$ mm^2 can be observed on the surface of the film which was processed with a cooling rate of 20 °C/h (Fig. 4a). Both types of crystallite growth were found on the surface of this film; the perpendicular *c*-axis grain growth can be found in Fig. 4b; however, the inclined *c*-axis grain growth can be observed in Fig. 4c. It is important to mention that the majority of the crystallites on the surface of films prepared by fast cooling rates were perpendicular *c*-axis grain growth but with slow cooling rates the majority of crystallites were inclined *c*-axis grain growth and this agrees with the XRD results.

The cross section optical micrographs for films processed by cooling rates of 100 °C/h and 20 °C/h are shown in Fig. 5a, b, respectively. The relatively dark areas in the film are the Nd_{123} phase while the light precipitates are the Nd_{422} phase (SEM-EDX analysis). Figure 5a can be characterized by a narrow interaction layer, multi-domain growth and the presence of a large number of small Nd_{422} particle sizes. In contrast, the use of 20 °C/h cooling rate has led to coarsening some of Nd_{422} particles and increasing the width of the interaction layer. It is interesting to note that the CuO precipitates in Fig. 5b are less than those in the processing of the YBCO system on YSZ substrate [2], although a longer time has elapsed at a high temperature in the processing of the NdBCO film. This reflects the importance of the Nd_{422} addition in the melt processing of NdBCO thick films.

Superconducting properties

The AC susceptibility of thick films processed by different cooling rates is shown in Fig. 6a. High-T_C and sharp superconducting transitions can be observed for all processed and oxygen annealed films T_C values and the corresponding transition widths (ΔT_C) as a function of the cooling rates are shown in Fig. 6b, together with the solubility limit *x* values calculated from the SEM-EDX analyses. T_C increases with decreasing cooling rate accompanied by a slight decrease in solubility. It is well known that the formation of the Nd_{123} high-T_C phase is preferred at a high temperature [15] and the slower cooling rate gives more time at the high temperature for the formation of the Nd_{123} high-T_C phase.

Since the processed films consisted of regions of perpendicular and inclined *c*-axis oriented Nd_{123} crystallites which are separated by high percentage regions of Nd_{422} phase, the measured overall J_C was low. Figure 7a shows the transport J_C of films processed at different cooling rates. It is important to mention that the values of J_C were measured across the whole film. The maximum J_C value was observed with cooling rates 120 °C/h and 100 °C/h. Although a high degree of perpendicular *c*-axis texturing was observed in the film prepared with a cooling rate of 140 °C/h, its

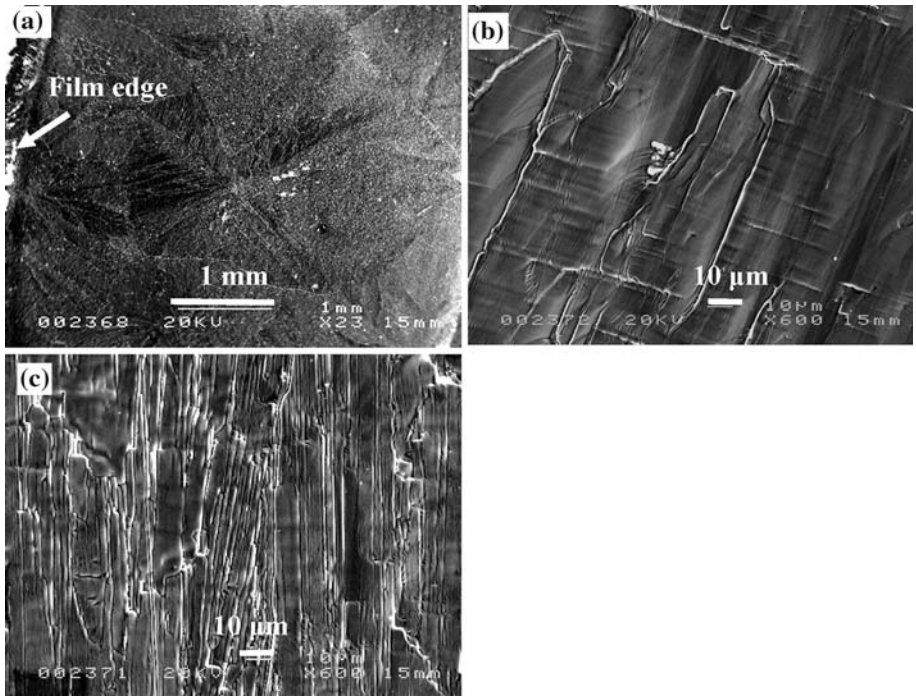

Fig. 4 SEM surface images of NdBCO thick films processed by a cooling rate of 20 °C/h

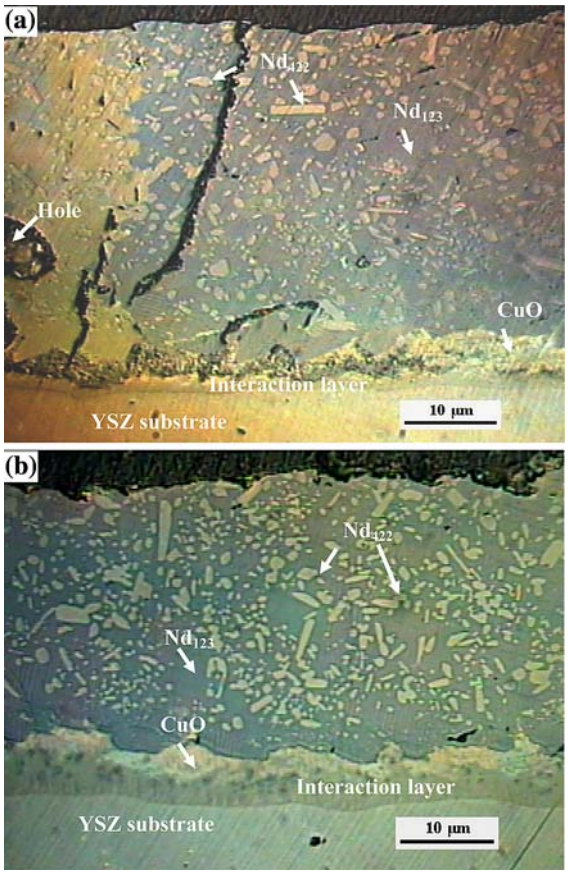

Fig. 5 Optical polished cross section photographs of thick films prepared by cooling rates: (**a**) 100 °C/h; (**b**) 20 °C/h

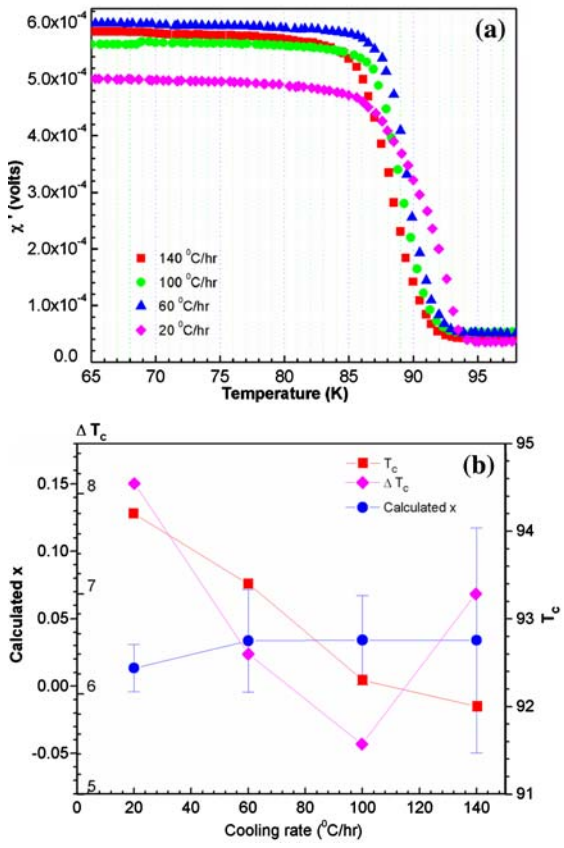

Fig. 6 (**a**) the temperature dependence of AC susceptibility of thick films processed by cooling rates 140, 100, 60 and 20 °C/h. (**b**) the change of T_C, ΔT_C and the calculated solubility limit x with the cooling rate

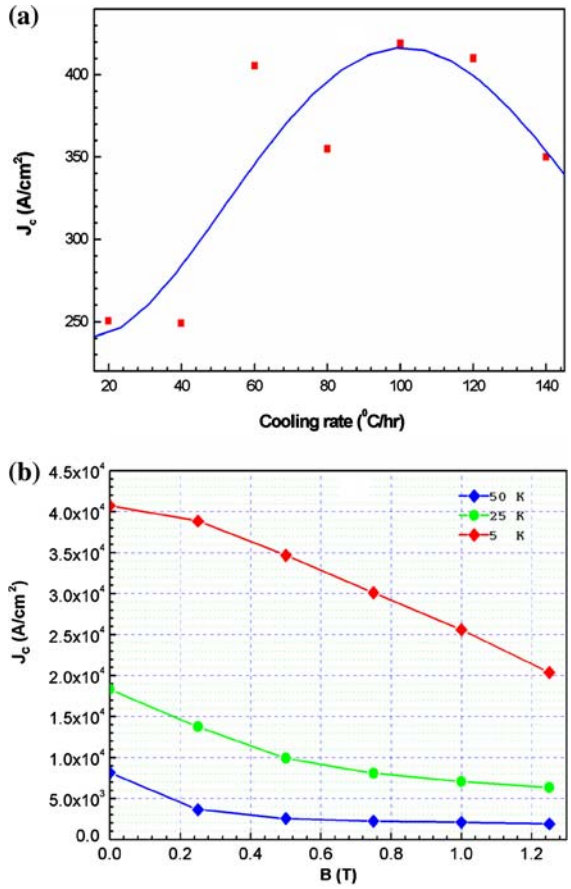

Fig. 7 (**a**) The zero field transport critical current density as a function of the cooling rate at 77 K. (**b**) the magnetization critical current density of the film which was prepared by a cooling rate of 20 °C/h at 5, 25 and 50 K under different applied magnetic fields

J_C is not as high when compared with the films prepared at 120 °C/h and 100 °C/h. This could be due to the formation of small crystallites (Fig. 3b). The value of J_C was reduced with 40 °C/h and 20 °C/h cooling rates, which could be due to the wide Nd_{422} area between the relatively large crystallites. To asses the critical current inside one large crystallite (cooling rate 20 °C/h), the largest crystallite in Fig 4a has been cut and used to measure the magnetization critical current by VSM technique. The magnetization of this crystallite was measured at 5, 25 and 50 K under different applied magnetic fields parallel to the film surface. The value of J_C was calculated using Bean model equation [28], $J_C = 30\Delta M/d$, where J_C (A/cm^2), ΔM is the hysteresis of the magnetization curve (emu/cm^3) and d is the sample dimension. Figure 7b shows the calculated J_C as a function of the magnetic field at 5, 25 and 50 K. The zero field values are all higher than the transport value in Fig. 7a due to the temperature difference and the fact that the magnetization measurements were taken on an individual crystallite. The weak-field dependence indicates strong pinning centres in the crystallite. As the temperature decreases the effectiveness of this enhanced flux pinning increases. It is well known that the presence of Nd_{422} enhances the flux pinning in the low-field and high-temperature region [29] and diminishes rapidly as the applied field increases. Conversely, slight chemical variations (Nd-rich clusters) appear to act as effective pinning centres at higher applied magnetic fields [15]. Consequently, it can be concluded that the flux pinning in this crystallite is due to the presence of Nd_{422} precipitates and Nd_{123SS} clusters.

MO and J_C measurements

Further investigation of the superconducting properties of the annealed films was undertaken using MO imaging. Figure 8a, b show the flux penetration behaviour of the 100 °C/h oxygen annealed film at 5 K and under applied magnetic field 14 mT and 29 mT, respectively. Figure 8c, d show the flux distribution at 10 K in the film cooled at 20 C/h for external fields 14 mT and 44 mT, respectively. The light colour represents flux penetration in the weak link areas, but the dark contrast regions, where the flux has not penetrated, reflect the shape of the Nd_{123} superconducting grains. As can be observed in Fig. 8a, b the fast cooling rate produces small grains which contain clear weak links. With a slower large 'butterfly like' grains were obtained (Fig. 8c, d). From the corresponding SEM images, the parallel weak links inside the grains are due to cracks. These cracks could come from the difference in thermal expansion between the film and substrate and/or from the tetragonal to orthorhombic transformation during the oxygen annealing. It is interesting to note that the majority of these cracks were observed after the oxygen annealing.

Conclusions

Although the deliberate presence of relatively large amount of unreacted precursor in the starting powder has decreased the melt viscosity, the addition of Nd_{422} has helped in stabilising the increased liquid amount for long time at high temperature and the use Ba-rich Nd_{123} has allowed high quality films with high T_C and large grain size to be grown. At higher cooling rates the films exhibit greater texture, smaller grains and a smaller reaction layer and higher transport J_C, but lower T_C than the films slowly cooled. However, the value of transport and magnetization J_Cs of these films has been degraded due to the presence of weak links

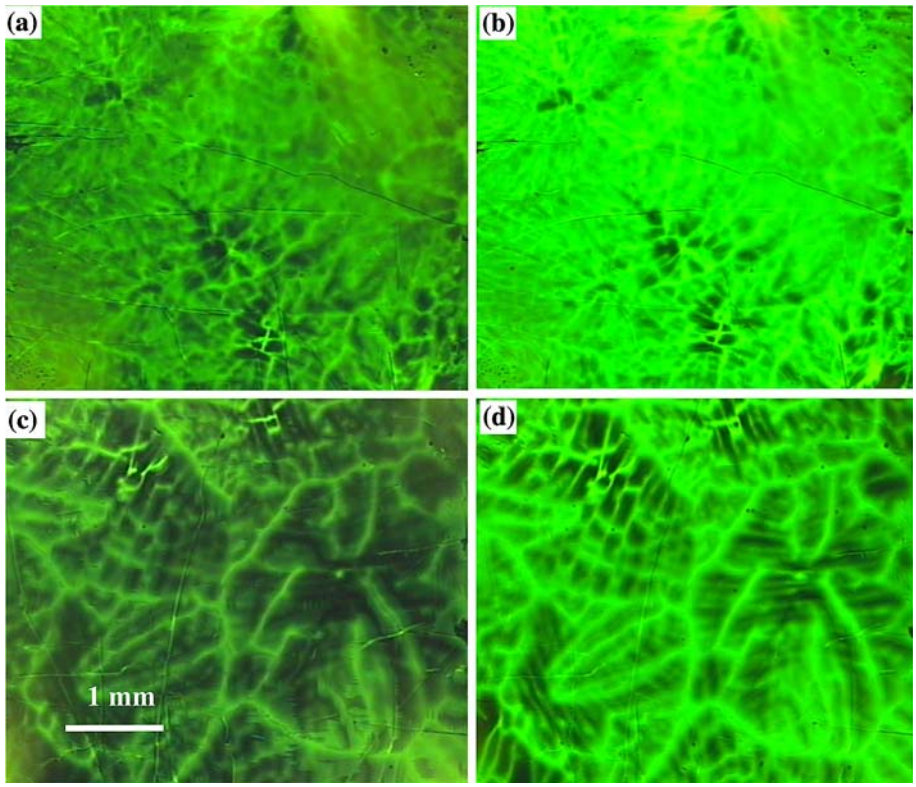

Fig. 8 (**a**) MO images of the NdBCO thick films processed by cooling rates 100 °C/h and 20 °C/h at different temperatures and under different applied magnetic fields: (**a**) and (**b**) cooling rate 100 °C/h at 5 K and under 14 mT and 29 mT, respectively; (**c**) and (**d**) 20 °C/h at 10 K and under 14 mT and 44 mT, respectively

between the crystallites and high density cracks inside the grains, respectively, as revealed by MO imaging.

References

1. Hashimoto T, Kosaka T, Yoshida Y, Fueki K, Koinuma H (1988) Jpn J Appl Phys 27(3):L384
2. Bi YJ, Wellhofer F, Day M, Abell JS (1993) Mater Sci Eng B 12:19
3. Day MJ, Sutton SD, Wellhofer F, Abell JS (1993) Supercond Sci Technol 6:96
4. Langhorn J, Bi YJ, Abell JS (1996) Physica C 271:164
5. Penn SJ, McN Alford N, Bracanovic D, Esmail AA, Scott V, Button TW (1999) IEEE Trans Appl Supercond 9:3070
6. Bracanovic D, Esmail AA, Pen SJ, Webb SJ, Button TW, McN Alford N (2001) IEEE Trans Appl Supercond 11:2422
7. Moule DJ, Evans PD, Shields TC, Foulds SAL, Price JPG, Abell JS (1997) IEEE Trans Appl Supercond 7:1025
8. Opie DB, Read ME, Remillard SK, Brown MJ, Kossler WJ, Schone HE, Button TW, McAlford N (1993) IEEE Trans Appl Supercond 3:189
9. Lancaster MJ, Maclean TSM, Niblett J, McN Alford N, Button TW (1993) IEEE Trans Appl Supercond 3:2903
10. McN Alford N, Penn SJ, Button TW (1997) Supercond Sci Technol 10:169
11. Wolf Th, Borbarel A-C, H Küpfer, Meier-Hirmer R, Obst B (1997) Phys Rev B 56:6308
12. Wolf Th, Küpfer H, Wühl H (1996) In: Matshushita T, Yamafuji K (eds) Proceedings of the 8th International Workshop on Critical Currents in Superconductors. Kitakyushu, Japan, World Scientific, Singapore, p 411
13. Salama K, Parikh AS, Woolf L (1996) Appl Phys Lett 68:1993
14. Takahashi M, Sakai N, Yoo SI, Murakami M (1996) In: Nakajima S, Murakami M (eds) Advances in Superconductivity IX. Springer, Berlin, p 713
15. Murakami M, Sakai N, Higuchi T, Yoo SI (1996) Supercond Sci Technol 9:1015
16. McCallum RW, Kramer MJ, Dennis KW, Park M, Wu H, Hofer R (1995) J Elect Mater 24:1931
17. Bieger W, Krabbes G, Schatzle P, Zelenina L, Wiesner U, Verges P, Klosowski J (1996) Physica C 257:46
18. Yoo SI, Sakai N, Takaichi T, Higuchi T, Murakami M (1994) Appl Phys Lett 65:633
19. Hu AM, Zhao ZX, Wu MZ, Wende C, Strasser T, Jung B, Bruchlos G, Gawalek W, Goernert P (1997) Physica C 278:43
20. Dimesso L, Marchetta M, Calestani G, Migiliori A, Masini M (1997) Supercond Sci Technol 10:347
21. Kojo H, Yoo SI, Murakami M (1997) Physica C 289:85
22. Shields TC, Riley A, Abell JS (1997) Inst Phys Conf Ser No 158:209
23. Dimesso L, Hyun OB, Hirabayshi I (1995) Physica C 248:127
24. Moussa MA, Abell JS, Shields TC (2002) Supercond Sci Technol 15:1467
25. Moussa MA, Abell JS Shields TC, Kawano K (2003) Supercond Sci Technol 16:617
26. Day MJ (1992) Fabrication, characterization of high-temperature superconducting thick films. Ch. 7, Ph. D. thesis, Birmingham University
27. Ingle NJC, Cardwell DA, Jones AR, Wellhofer F, Button TW (1995) Supercond Sci Technol 8:282
28. Bean CP (1962) Phys Rev Lett 8:250
29. Mochida T, Chikumoto N, Murakami M (2000) Phys Rev B 62:1350